JOINT INSTITUTE FOR NUCLEAR RESEARCH
Veksler and Baldin laboratory of High Energy Physics

FINAL REPORT ON THE START PROGRAMME

Analysis of the Irradiation of CR-39 Solid-State Nuclear Track Detector with a ^{124}Xe Beam at 3.85 A GeV

Supervisor:
Dr. Pavel Zarubin

Student:
Stanislau Murashka, Belarus
Belarusian State University

Participation period:
February 22 – March 11,
Winter Session 2023

Dubna, 2023

Abstract

The goal of the work was to analyse the results of irradiation of CR-39 solid-state nuclear track detector (SSNTD) by ^{124}Xe beam of the 3.85 A GeV kinetic energy at the BM@N installation in the 4th Commissioning Run of the NICA Complex. The work also included studying the technique of using SSNTD in the beams of relativistic Xenon nuclei at the Nuclotron-NICA accelerator complex. The Olympus BX63 motorised microscope was applied to scan the detector surface in the beam area. Based on this scan, the formed tracks were analysed and the Xenon beam profile was evaluated.

Introduction

The method of using the solid-state nuclear track detectors (SSNTDs) is one of the methods of ion beam profilometry, which is based on application of solid-state materials able to detect traces of ions passing through them. When ions interact with solid-state material, tracks are formed whose location and shape depend on the energy, type of ions and angle of incidence. By measuring the parameters of the tracks on the surface of a solid-state detector, it is possible to obtain information about the distribution of ion charges in a monoenergetic beam [1,2].

The SSNTD method has some advantages over other profilometry methods, such as high spatial resolution, absence of the detector dead time, and low cost. This justifies an opportunity of using SSNTDs to monitor the density, position and total intensity of the heavy relativistic ion beam.

This study was carried out in the framework of irradiation in the beam of ^{124}Xe, accelerated for the first time at the JINR Nuclotron in December 2022, stacks of nuclear emulsion according to the BECQUEREL experiment [3].

The aim of the above project is to master the applications of Solid-State Nuclear Track Detectors in beams of Xenon relativistic nuclei at the NICA accelerator complex.

1. NICA acceleration complex

Nuclotron-based Ion Collider fAcility (NICA) is an accelerator complex which is under construction at the Joint Institute for Nuclear Research to study properties of dense baryonic matter. NICA goals cover many domains including research of the nature and properties of strong interactions between elementary constituents of the Standard Model, search for signs of the phase transition between hadronic matter and quark-gluon plasma, search for new phases of baryonic matter and study of basic properties of the strong interaction vacuum and QCD symmetries [4].

The NICA complex consists of the following parts: (the scheme of the complex is shown in Figure 1)

1. injection complex
2. superconducting Booster synchrotron
3. superconducting heavy ion synchrotron called Nuclotron
4. collider
5. beam transfer channels
6. BM@N, SPD and MPD detectors

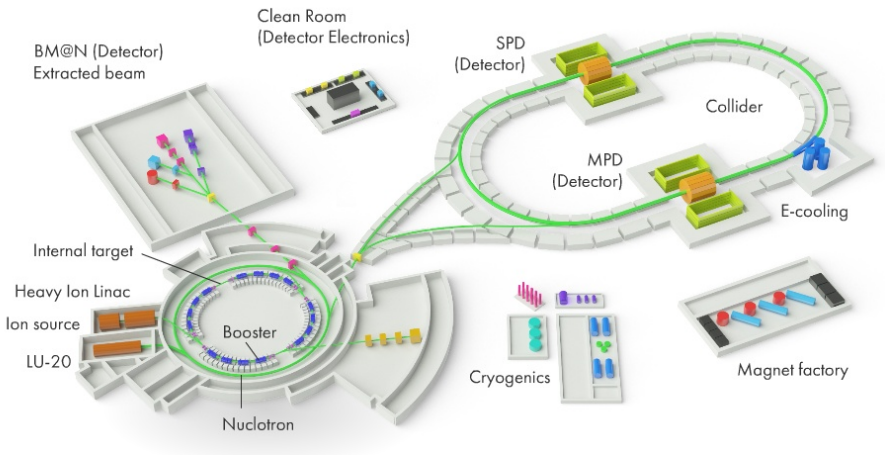

Figure 1: The NICA complex [4].

The NICA booster is an accelerator with 211 m of circumference and four-fold symmetry lattice inside the yoke of the Synchrophasotron. It will accelerate beams to 500 MeV and use the 2.2 m-long dipole and quadrupole magnets. The task of the booster is to accumulate ions and accelerate the ions up to the energy required for efficient stripping; forming the required beam emittance with the electron cooling system and providing fast extraction of the accelerated beam for its injection into the Nuclotron [4].

The Nuclotron SC proton synchrotron has three operational modes:

1. Acceleration of heavy ions for the storage in the collider.
2. Acceleration of polarised protons and deuterons for feeding the collider.
3. Acceleration of both polarised and unpolarized protons and deuterons and heavy ions for internal target experiments or slow extraction to the fixed target experiments [4].

2. Materials and methods

CR-39 LET spectrometer is based on a poly(allyl diglycol carbonate) (PADC) track detector; the chemical formula and structure of its monomer is $C_{12}H_{18}O_7$. PADC is a clear, rigid plastic with density of about 1.30 g·cm^{-3}. This material is one of the most sensitive track detector materials and it can directly register energetic protons, alpha particles, and heavier nuclei [1,2].

A heavy ion passes through the CR-39 causing radiation damage which is called the latent track. To observe the tracks using an optical microscopy, it is needed to enlarge them by chemical etching of the detector. A chemical etchant will erode the radiation damage region more rapidly than in the undamaged region. The former and latter erosion rates are respectively called: the track etch rate (V_t) and bulk etch rate (V_b). Due to the erosion of the latent track, a conical etched pit appears in the detector material (see Figure 2) [5].

The rates V_b and V_t depend on the following parameters: chemical composition of the detector, etching conditions such as temperature, composition and concentration of the etching solution and the presence of stirring. Also, the bulk etching rate depends on the irradiation dose of the detector before etching with different kinds of ionising radiation [5].

For CR-39 typical chemical etchants are solutions of NaOH and KOH. The etching rate and time are selected taking into account the investigated linear energy transfer and particle fluence.

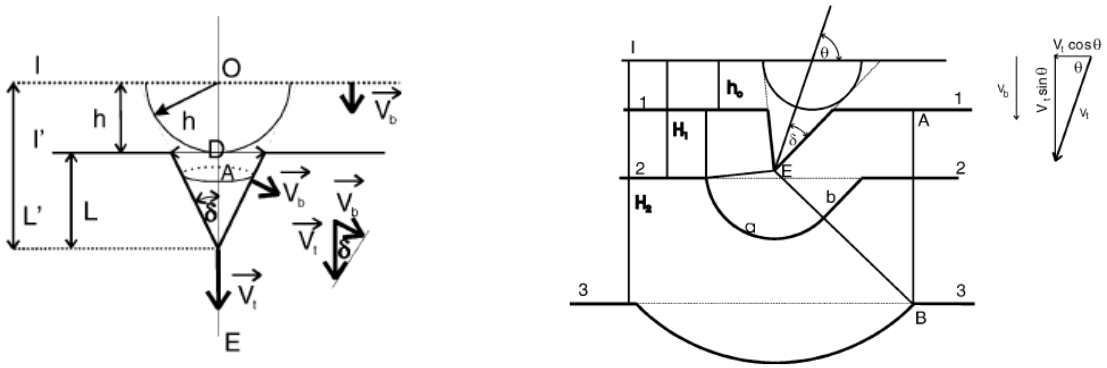

Figure 2: Geometry of the track development with constant ***Vt***. On the right side, the path of the particle ends at point E [5].

The track registration sensitivity (S) is defined as the reduced etching rate ($S = V_t/V_b - 1$), and it depends on the ionisation energy loss including δ-electrons. However, high-energy δ-electrons carry the energy away and do not contribute to latent track formation. For CR-39 minimum linear energy transfer at which track formation occurs is about 3 keV/μm [1,2,6].

Then, S can be converted into LET using a conversion function which varies depending on the manufacturer of the CR-39 and etching conditions [5,7].

3. Experiment

Irradiation of CR-39 detector was carried out on the experimental installation Baryonic Matter at Nucleotron (BM@N) in the 4th Commissioning Run at the NICA Complex. The energy of the ^{124}Xe beam was 3.85 A GeV, and the expected loading of the detector was 5 spills of the order of 10^6 ions. The detector was located between the time-of-flight mRPC system and the zero degree calorimeter (Figure 3), while the surface normal of the CR-39 coincided with the beam direction.

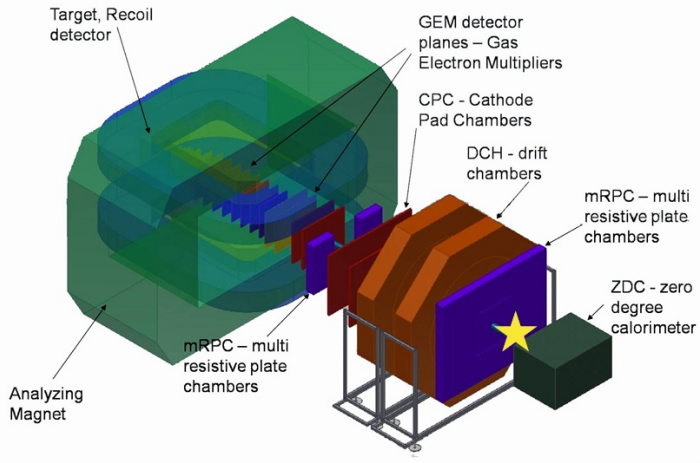

Figure 3: Scheme of the BM@N experimental setup. An asterisk indicates the location of the SSNTD CR-39 [4].

The investigated CR-39 detector was a 50x50 mm plate 1 mm thick initially. After irradiation, the CR-39 sample was etched in an aqueous solution of 6M NaOH. The system was in a thermostat maintaining the temperature equal to 85 °C with an accuracy of 0.1 °C. The etching time was 20 minutes.

4. Scanning the detector on the microscope

Figure 4 shows the zone of CR-39 that got under the ion beam. The turbidity of the plastic is caused by light scattering of a large number of the etched tracks.

Figure 4: Appearance of the irradiated and etched area of SSNTD CR-39. The region of turbidity corresponds to the passage of the beam.

Scanning was carried out by means of a unique motorised microscope Olympus BX63 (Figure 5) using proprietary software Olympus cellSens which fulfils the acquisition of panoramic images while manual scanning or in automatic mode with focus maps. Also, within the framework of this program, an automatic search is carried out for objects in the image.

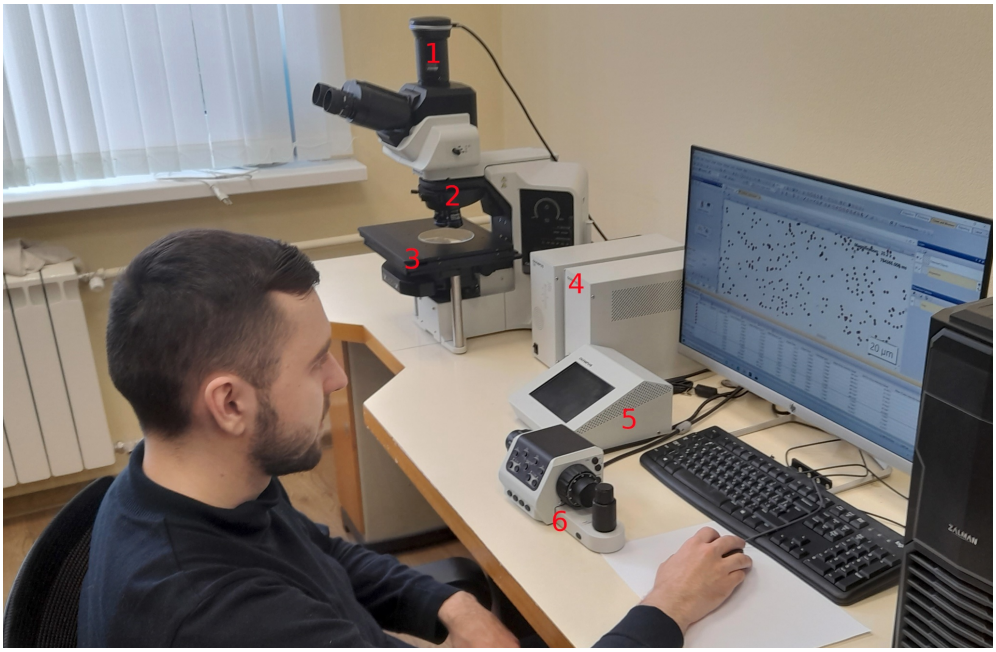

Figure 5: Olympus BX63 motorised microscope. 1) microscope camera, 2) lens revolver, 3) motorised stage, 4) microscope control units, 5) controller, 6) touch panel controller.

During irradiation, the angle of incidence of Xe ions was close to perpendicular, which resulted in forming the tracks which approximately had a circular shape. The track images obtained using 4x, 20x, and 40x objectives are shown in Figures 6, 7, and 8, respectively.

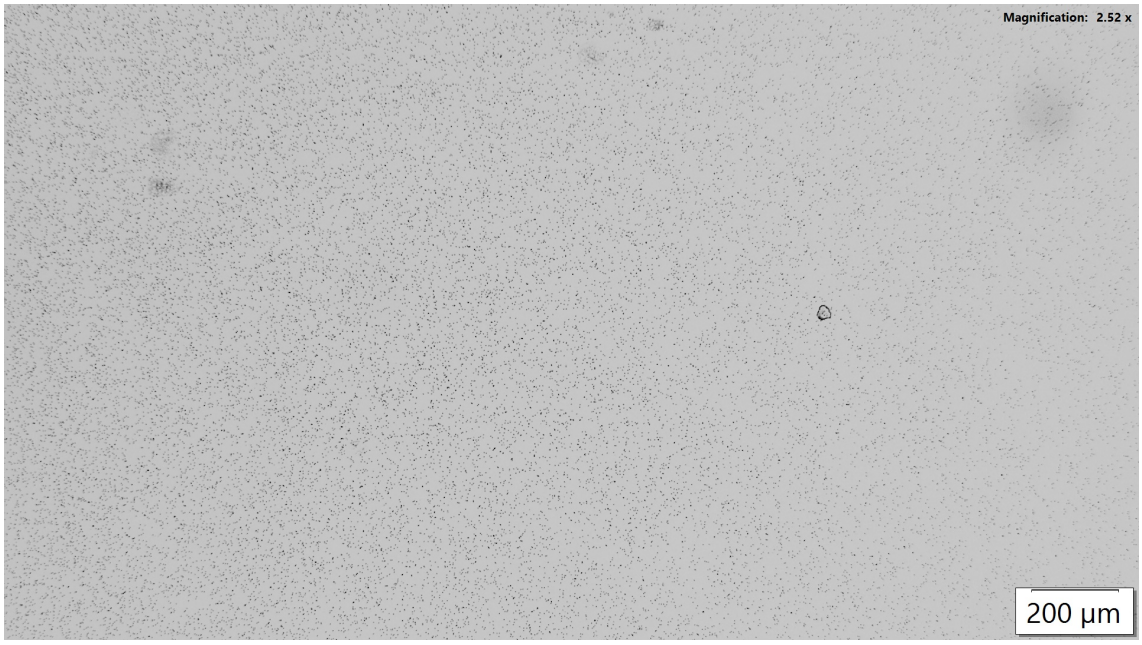

Figure 6: Photo of CR-39 SSNTD at the intermediate beam density, taken with the Olympus BX63 microscope using a 4x objective.

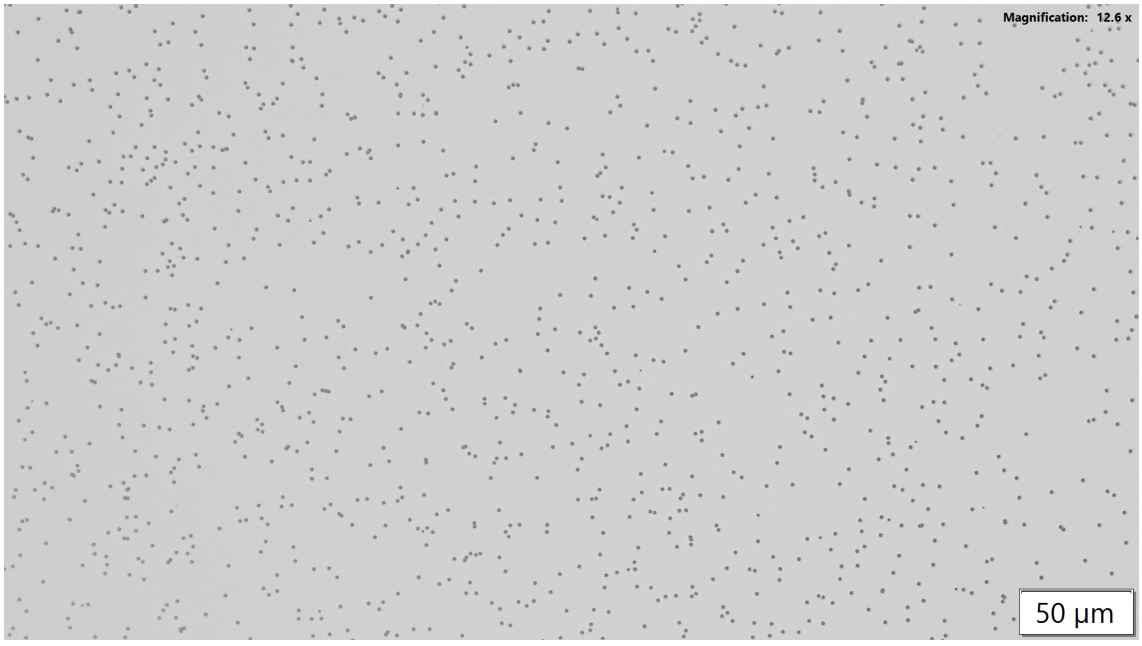

Figure 7: Photo of CR-39 SSNTD at the intermediate beam density, taken with the Olympus BX63 microscope using a 20x objective.

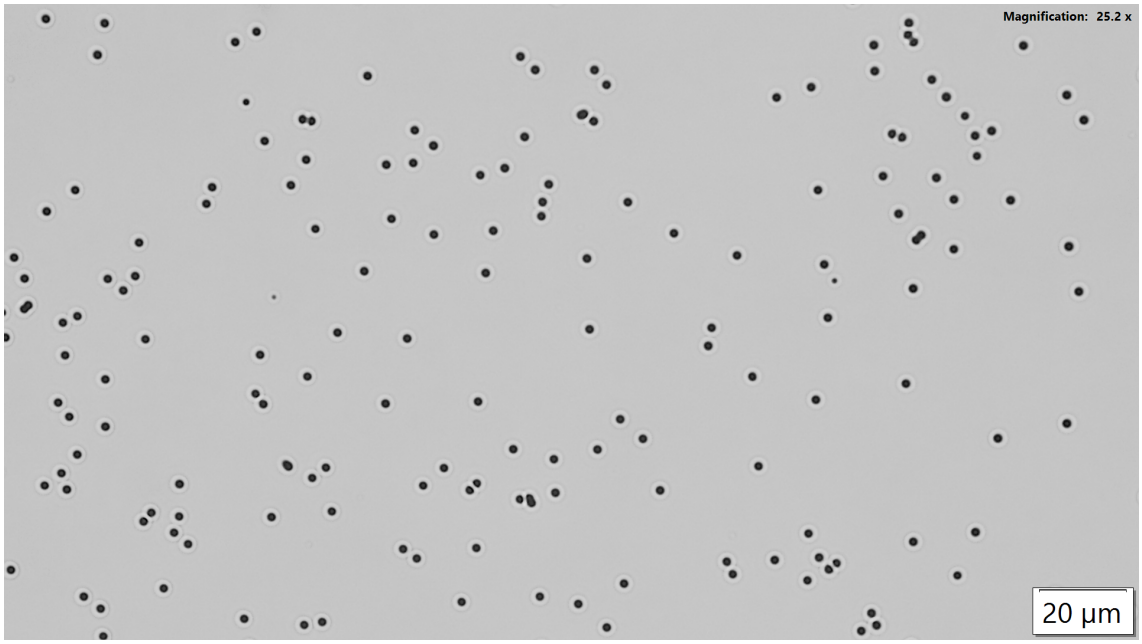

Figure 8: Photo of CR-39 SSNTD at the intermediate beam density, taken with the Olympus BX63 microscope using a 40x objective.

In the framework of this study, the selection of dip (depressions formed as a result of etching the latent areas of the detector) in the images was carried out according to the gray level. After that the information about the objects, including their position in the image, a mean radius, area, aspect ratio and other characteristics, was recorded in the Table (see Figure 9). In addition, random plastic defects were recorded during the experiments.

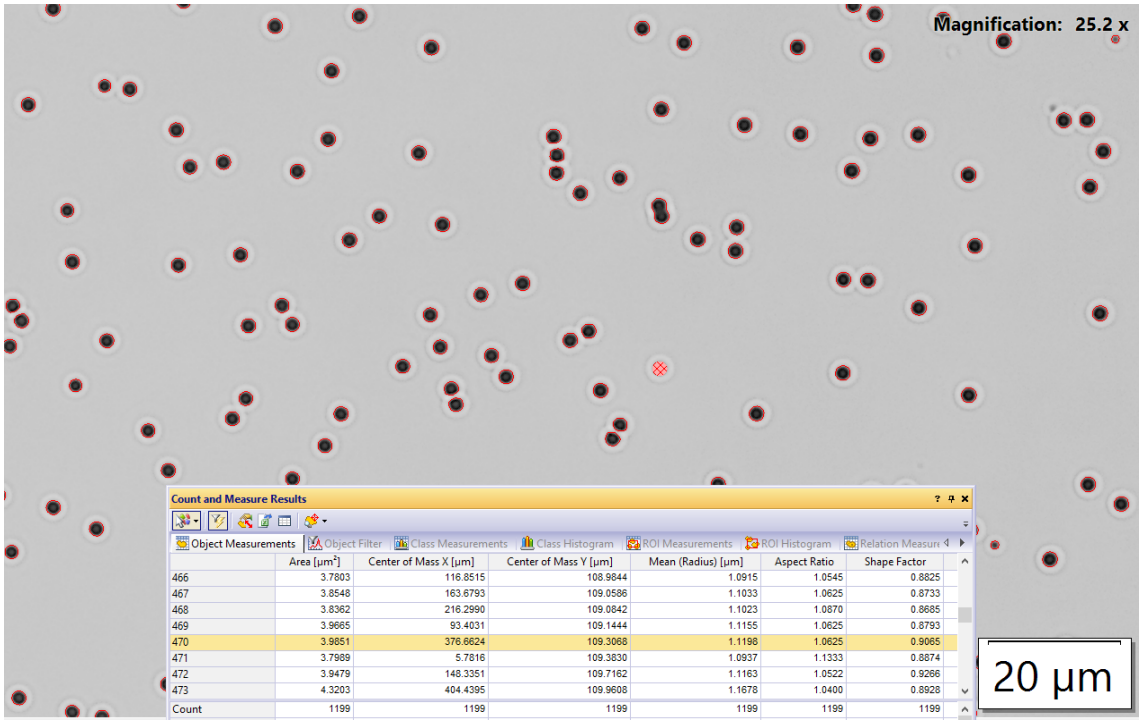

Figure 9: Image of objects recognized by the Olympus cellSens software on a SSNTD CR-39 using a 40x objective.

It is worth emphasising that attempts of automatically scanning the entire area using the proprietary software have not given any results. The reason was the roughness of the plastic surface, which resulted in tracks leaving the working range of the lens even when using a focus map. At the same time, the operation of the auto focus implemented in cellSens turned out to be unreliable.

In order to optimise the manual digitization time, the surface was scanned with a 40x lens by means of the automatic panoramic image stitching function, using the focus map. In this case, the size of the panorama was chosen to be equal to 24000 x 24000 pixels, that corresponds to a square with an area of 10.7 mm^2 and a width of 136 nm/pixel.

5. Data processing

After image processing, the tables with dip parameters were obtained for each panorama. When combining the obtained tables into one dataset, the information was deduplicated to eliminate the same tracks caused by photo overlapping. The total number of the registered objects is approximately equal to $2.5 \cdot 10^6$.

In Figures 10 and 11, the black lines show the distributions of the mean radius and dip areas whose spread out is partially caused by defocusing due to the roughness of the detector surface. Several vertices of the curves can be observed in the presented images, which, probably, arose in part due to track overlapping.

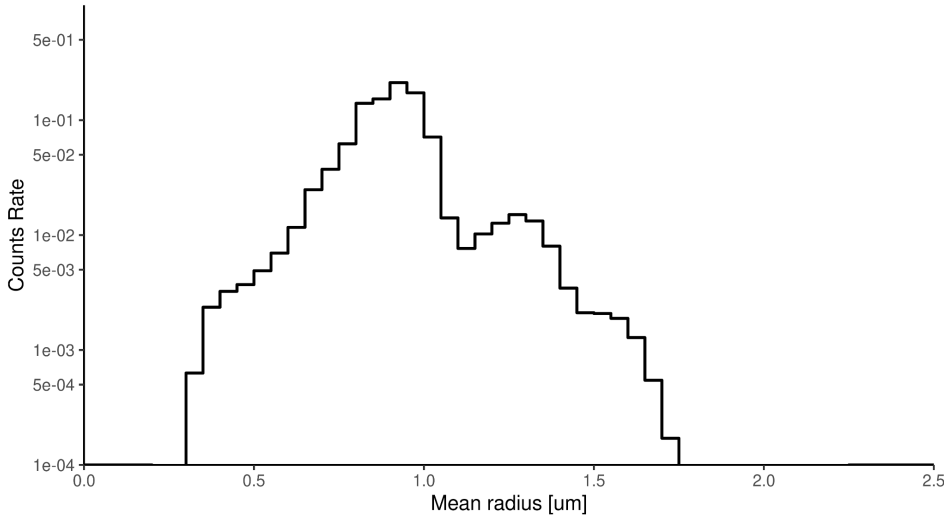

Figure 10: Distribution of the mean radius of the registered objects over the entire area of the detector.

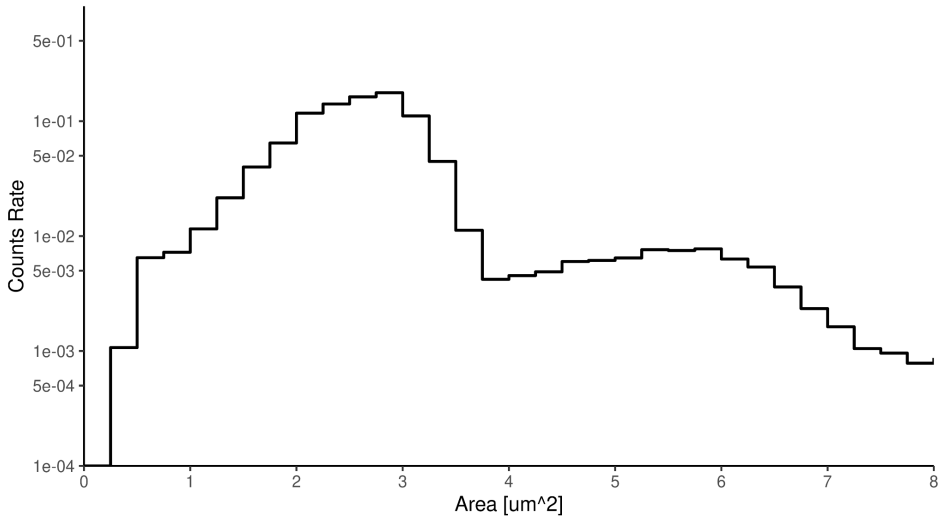

Figure 11: Distribution of areas of the registered objects over the entire area of the detector.

Figures 12 and 13 show the result of separating the events according to the aspect ratio of the rectangle *AR* that describes them. If we assume that objects with an aspect ratio *AR* greater than 1.25 are formed by overlapping of two or more tracks, then the peaks of the average radius and area distributions indicated in the Figures by the dotted lines, will correspond to the track overlapping. It should be noted that due to the pixelization of the round track images, their aspect ratio values may slightly exceed 1.

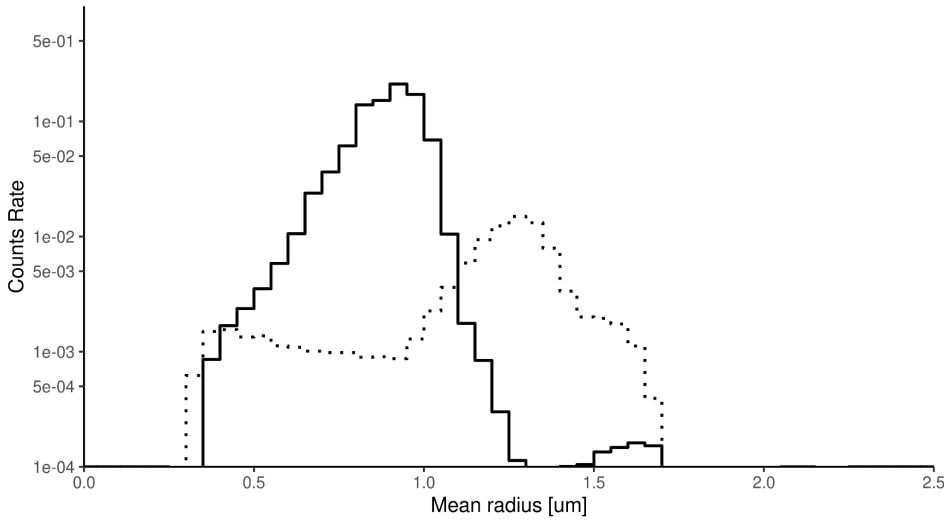

Figure 12: Distribution of the mean radius of the registered objects over the entire area of the detector. The solid line corresponds to the objects with *AR* not exceeding 1.25, the dotted line corresponds to *AR* > 1.25.

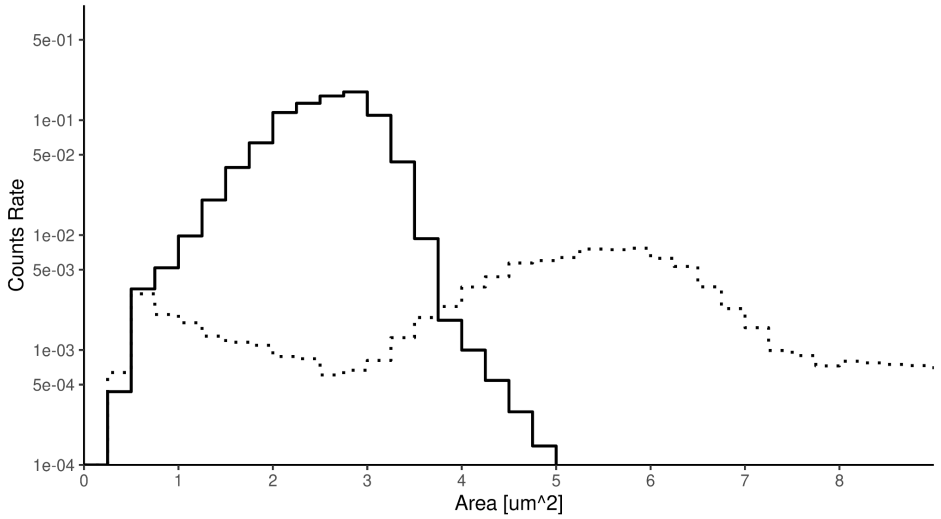

Figure 13: Distribution of areas of the registered objects over the entire square of the detector. The solid line corresponds to objects with *AR* not exceeding 1.25, the dotted line corresponds to *AR* > 1.25.

The final distribution of the number of counts by coordinates is shown in Figure 14. At the top (y ~ 20000 μm) of the right edge plot, there is a number of the registered plastic fragments.

The gap at the lower edge of the plot is caused due to the engraving of the inscription. The main region of the beam has an elliptical shape with an inclination of the ellipse of about 45°. The beam ellipse, inside which the density dip exceeds 10^3 mm^{-2}, has the dimensions of the major and minor semi axes of the order of 16 and 8 mm, respectively.

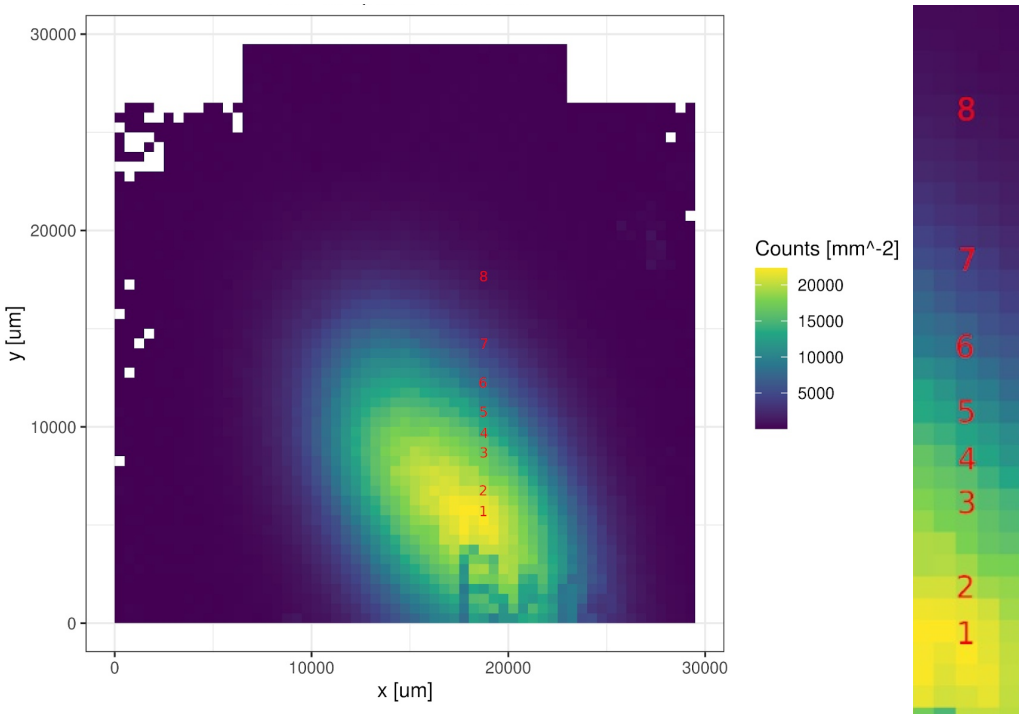

Figure 14: Spatial distribution of dip over the area of the CR-39 SSNTD. The bin width is 0.5 mm. On the right there are the centres of the analysed squares.

6. Visual counting of the number of tracks.

In the process of registration, two or more track overlappings were recorded as single events. Therefore, when determining the number of tracks, the presence of these overlapped events must be taken into account. To estimate the frequency of overlapping tracks by means of the visual method, several squared areas of the detector were selected (Figure 14), where the frequencies of formation of double f_d (Table 1) and triple f_t (Table 2) tracks were manually calculated visually. The binomial distribution function *pbinom* implemented in the *stats* package (version 4.0.4) was applied to calculate the confidence interval [8].

Table 1. Number of events for overlapping 2 tracks.

No. Square	Square side [mm]	Total number of dips	Number of dips normalised to 1 mm^2	Number of double tracks	Sampling frequency f_d	95% confidence interval f_d	1 - 10^{-6} confidence interval f_d
1	0.25	1370	21920	163	0.11898	[0.10298; 0.13739]	[0.08098; 0.16668]
2	0.25	1288	20608	157	0.12189	[0.10524; 0.14102]	[0.08245; 0.17160]
3	0.25	1110	17760	112	0.10090	[0.08464; 0.12014]	[0.06289; 0.15141]
4	0.25	982	15712	71	0.07230	[0.05781; 0.09033]	[0.03919; 0.12044]
5	0.25	744	11904	28	0.03763	[0.02626; 0.05393]	[0.01332; 0.08313]
6	0.25	502	8032	24	0.04781	[0.03248; 0.07030]	[0.01544, 0.11072]
7	0.5	980	3920	11	0.01122	[0.00634; 0.01999]	[0.00186; 0.03735]
8	1	772	772	0	0	[0; 0.00477]	[0; 0.01862]

Table 2. Number of events for 3 overlapped tracks.

No. Square	Square side [mm]	Total number of dips	Number of dips normalised to 1 mm^2	Number of triple tracks	Sampling frequency f_t	95% confidence interval f_t	1 - 10^{-6} confidence interval f_t
1	0.25	1370	21920	34	0.02482	[0.01782; 0.03452]	[0.00972; 0.05182]
2	0.25	1288	20608	21	0.01630	[0.01073; 0.02482]	[0.00476; 0.04063]
3	0.25	1110	17760	14	0.01261	[0.00758; 0.02107]	[0.00265; 0.03741]
4	0.25	982	15712	12	0.01222	[0.00707; 0.02125]	[0.00222; 0.03894]
5	0.25	744	11904	2	0.00269	[0.00083; 0.00968]	[0.00002; 0.02642]
6	0.25	502	8032	1	0.00199	[0.00048; 0.01105]	[0, 0.03414]
7	0.5	980	3920	0	0	[0; 0.00376]	[0; 0.01470]
8	1	772	772	0	0	[0; 0.00477]	[0; 0.01862]

Further, according to the data in Tables 1 and 2, the number of tracks for each of the studied squares was calculated. The calculation results are presented in Table 3.

Table 3. Estimation of track density by the visual method.

No. Square	Square side [mm]	Total number of dips	Number of tracks	ratio of tracks to dips	Fluence [mm^{-2}]
1	0.25	1370	1601	1.16862	25616
2	0.25	1288	1487	1.15450	23792
3	0.25	1110	1250	1.12613	20000
4	0.25	982	1077	1.09674	17232
5	0.25	744	776	1.04301	12416
6	0.25	502	528	1.05179	8448
7	0.5	980	991	1.01122	3964
8	1	772	772	1.00000	772

7. Estimation of the probability of overlapping tracks with Monte Carlo

Figure 15 shows the distribution of the mean radius of the single tracks, obtained by means of manual photography of the CR-39. The values of the mean and standard deviation of the approximated Gaussian curve was $9.823(4)\cdot10^{-1}$ um and $2.082(3)\cdot10^{-2}$ um, respectively.

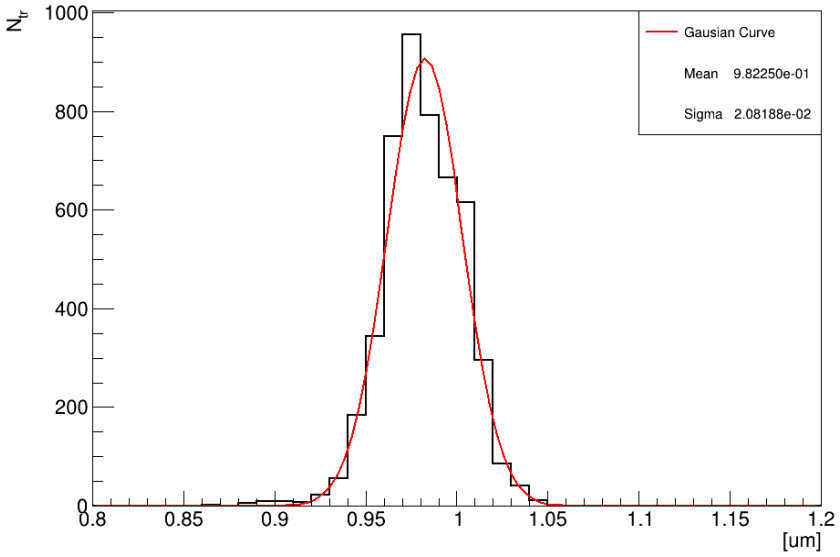

Figure 15: Distribution of the dip mean radius obtained from manual photography.

In the calculations, the track model was a circle, whose radius was set by the Gaussian random number generator with the parameters corresponding to Figure 15. The coordinates were generated by an isotropic distribution, while the coordinate plane had a square shape. The overlapping of two tracks was considered to be the event where the distance between the centres of the circles was less than the sum of the corresponding radii or equal to it. Due to the limited coordinate area, the overlap check was performed for the tracks located in the area obtained by the offset from the boundaries. In this case, the deviation from each boundary was 7 sums of the mean radius with 5 sigma.

Table 4 shows the frequency distribution of the number of tracks in one dip depending on the fluence. Due to fluctuations caused by offset from the edge of the coordinate area, the sample size was 1.0-1.1 million tracks.

Table 4. Frequency distribution of the number of tracks contained in 1 dip, calculated by the Monte Carlo method.

Fluence (mm^{-2})	dip per sq.mm	n=1	n=2	n=3	n=4	n=5	n=6	n>6
1000	993.98	9.940E-01	5.959E-03	5.501E-05	0	0	0	0
5000	4849.9	9.701E-01	2.882E-02	1.033E-03	4.603E-05	2.046E-06	0	0
10000	9411.2	9.417E-01	5.413E-02	3.845E-03	2.985E-04	2.329E-05	1.058E-06	0
15000	13687	9.139E-01	7.700E-02	7.936E-03	9.940E-04	1.202E-04	1.420E-05	2.185E-06
20000	17689	8.868E-01	9.771E-02	1.314E-02	1.965E-03	2.982E-04	4.051E-05	9.003E-06
25000	21444	8.614E-01	1.155E-01	1.882E-02	3.414E-03	6.677E-04	1.136E-04	3.362E-05
30000	24940	8.364E-01	1.317E-01	2.514E-02	5.324E-03	1.129E-03	2.649E-04	8.353E-05
35000	28166	8.124E-01	1.451E-01	3.199E-02	7.810E-03	1.963E-03	5.631E-04	1.972E-04
40000	31179	7.886E-01	1.580E-01	3.870E-02	1.042E-02	2.969E-03	8.900E-04	3.601E-04

In the future, it is planned to use the frequency distribution of the number of tracks to convert the number of dip into fluence.

Summary

In this paper, we have analysed the irradiation of CR-39 solid-state nuclear track detectors in the beam of Xe nuclei at A 3.85 GeV with 5 cycles of about 10^6 nuclei each over the expected area of about 1 sq. cm. The main results and conclusions are as follows:

1. CR-39 SSNTD was scanned over an area of 29.5 by 29.5 mm on a motorised microscope Olympus BX63. The total volume of digitised images in the compressed form was 1.6 GB.

2. According to the brightness of the found objects, dips were counted on the entire scanned surface. The proportion of dips consisting of two tracks for fluences of about $12.5 \cdot 10^3$ and $20 \cdot 10^3$ mm^{-2}, is about 4% and 10%, respectively. And the proportion of triple tracks is about 0.3% and 1.2%, respectively.

3. Based on the resulting array of measurements, the beam profile was reconstructed. It has an elliptical shape with an inclination of the ellipse of about 45 degrees. At the centre of the beam, the fluence was about $2.6 \cdot 10^4$ mm^{-2}. The main part of the beam accounts for approximately 1 sq. cm and fits into an ellipse with dimensions of the major and minor semi axes of the order of 16 and 8 mm, respectively.

4. The results obtained give grounds to use SSNTD CR-39 for beam monitoring while irradiating the stacks of nuclear emulsions and other objects.

5. On the whole, the performed analysis has indicated the prospects for using the SSNTD CR-39 in combination with a motorised microscope and the image analysis program in fundamental physical and radiobiological research.

Of further interest is the study of irradiating Mylar SSNTD with relativistic Xenon nuclei, and irradiation of SSNTD CR-39 at the energy of 3.2 A MeV with the Xenon beam at the SOChI workstation of the Nuclotron injector, as well as with the biomedical ^{12}C beam at the accelerator of the High Energy Physics Institute in Protvino.

References

1. Пикуз мл. С.А., Скобелев И.Ю., Фаенов А.Я., Лавриненко Я.С., Беляев В.С., Клюшников В.Ю., Матафонов А.П., Русецкий А.С., Рязанцев С.Н., Бахмутова А.В. Твердотельные трековые детекторы в исследованиях лазерной плазмы, Теплофизика высоких температур. 2016. Т. 54. № 3. С. 453-474.

2. Jadrníčková, I. & Spurný, F. & Molokanov, Aleksandr. (2008). Spectrometry of linear energy transfer and its use in high-energy particle beams. Physics of Particles and Nuclei Letters. 5. 531-537.

3. http://becquerel.jinr.ru/

4. https://nica.jinr.ru/

5. Nikezic, Dragoslav & Yu, Peter. (2004). Formation and growth of tracks in nuclear track materials. Materials Science & Engineering R-reports - MAT SCI ENG R. 46. 51-123.

6. Kodaira, Satoshi & Yasuda, Nakahiro & Kawashima, Hajime & Kurano, M. & Hasebe, Nobuyuki & Doke, T. & Ota, S. & Ogura, K. (2009). Control of the detection threshold of CR-39 PNTD for measuring ultra heavy nuclei in galactic cosmic rays. Radiation Measurements. 44. 861-864.

7. Kodaira, Satoshi & Morishige, K. & Kawashima, Hajime & Kitamura, H. & Kurano, M. & Hasebe, Nobuyuki & Koguchi, Yasuhiro & Shinozaki, W. & Ogura, Koichi. (2016). A performance test of a new high-surface-quality and high-sensitivity CR-39 plastic nuclear track detector – TechnoTrak. Nuclear Instruments and Methods in Physics Research Section B: Beam Interactions with Materials and Atoms. 383. 129-135.

8. R Core Team (2021). R: A language and environment for statistical computing. R Foundation for Statistical Computing, Vienna, Austria.